X-RAY DIFFRACTION IMAGING (TOPOGRAPHY) OF ELECTROOPTIC CRYSTALS BY SYNCHROTRON RADIATION

Bruce Steiner, Masao Kuriyama, Ronald C. Dobbyn, Uri Laor[1], National Bureau of Standards, Gaithersburg, Maryland 20899

The information of special interest to crystal growers and device physicists now available from monochromatic synchrotron diffraction imaging (topography) is reviewed. Illustrations are taken from a variety of electrooptic crystals. Aspects of the detailed understanding of crystal growth processes that can be obtained from carefully selected samples are described. Finally, new experimental opportunities now available for exploitation are indicated.

I. TYPES OF INFORMATION AVAILABLE

In contrast to electron microscopy, which provides information on the location of features in small regions of materials, diffraction imaging can portray minute deviations from crystal perfection over larger areas. Diffraction imaging by synchrotron x-radiation highlights irregularities that can affect performance. For example, lattice strains lead to strong contrast in such images, as in Figure 1; and analysis of the patterns in these strains can lead to a detailed understanding of how they arise[2]. Similarly, crystallographic dislocations, either alone or in arrays, also stand out in sharp contrast in the images of high quality crystals, as in Figure 2.

Analysis of such imperfections can lead not only to a detailed tally of their presence and distribution but also to an understanding of their origins and of steps that can be taken to reduce their presence. Thus, diffraction imaging provides useful information on the imperfections in high quality crystals that can be correlated with specific aspects of their performance and can lead to improvement in this performance through guidance on desirable modification in crystal growth parameters.

Synchrotron storage rings now permit far more comprehensive and useful realization of these possibilities than can be achieved with laboratory sources because of two optical characteristics of such rings: their effective small source size and their high brightness.

The small size leads to formation of highly parallel x-ray beams, which are required for maximum resolution. The smallest source size achieved to date, 140 micrometers, has been realized on the large storage ring at the National Synchrotron Light Source at Brookhaven National Laboratory. Optics at the end of one of its 20 meter beam lines thus can achieve at least 1.5 arc second angular resolution, or less than a micrometer on the surface of a detector in a typical configuration. This resolution can be further increased by the choice of optics. With appropriate optics, [illegible] resolution of individual dislocations is possible, as in Figure 3.

The high brightness achieved in storage rings is central to two aspects of crystal characterization. First, high brightness permits observation of diffraction features in transmission. The distinctive signatures of the dislocations observed in Figure 3 are visible only in diffraction in Laue geometry (transmission), with its integration of information from the interior of a crystal. Moreover, when strains are observed in transmission, as in Figure 4, differences in their direction in various parts of the image can be emphasized. In Figure

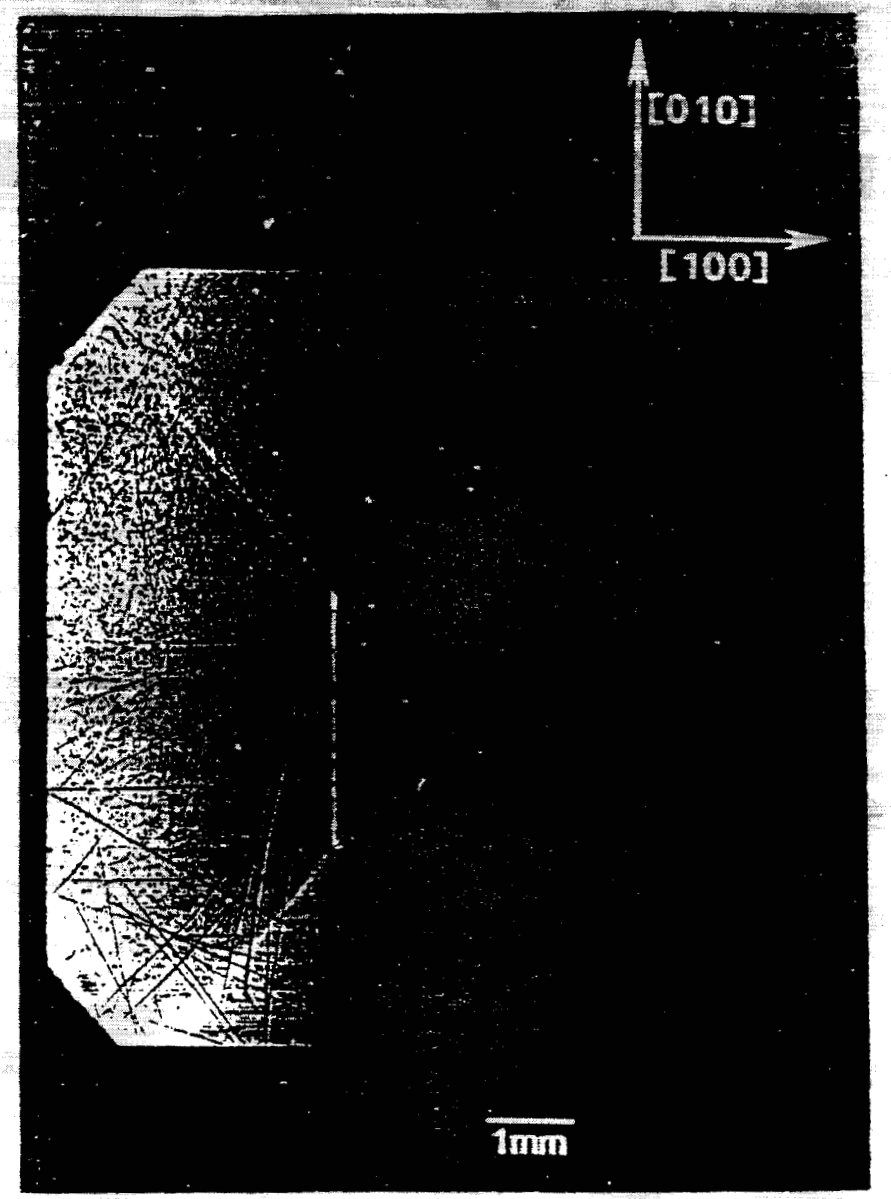

Figure 1. Strain patterns in the 8 keV (309) diffraction from a (001)-cut crystal (#K) of bismuth silicon oxide.

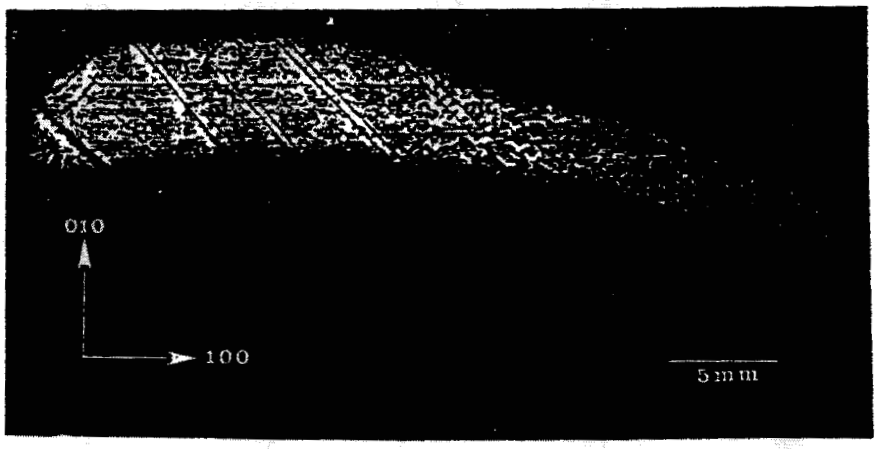

Figure 2. Dislocation patterns in the 10 keV (040) diffraction from an indium doped (001)-cut wafer of gallium arsenide.

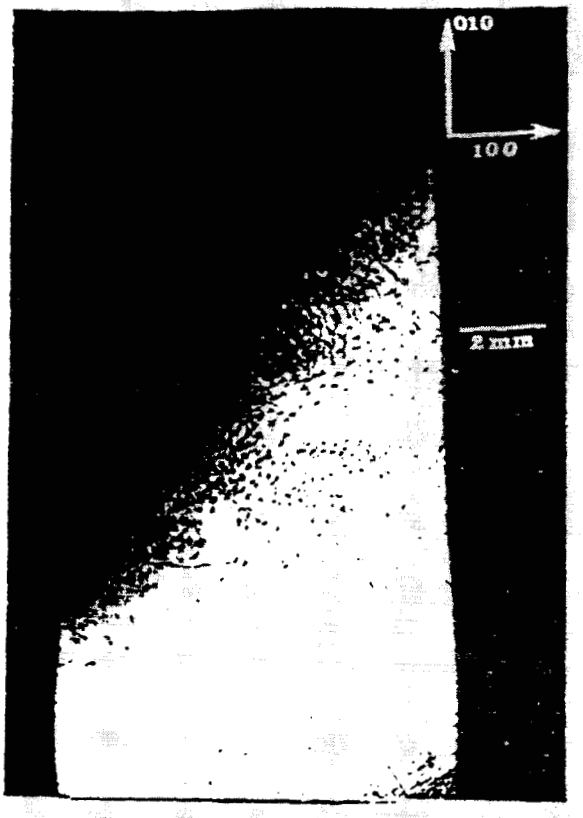

Figure 3. Individual dislocations resolved in 8 keV (400) diffraction from the indium doped (001) cut wafer of gallium arsenide shown in the previous figure, after fracture.

4, for example, strains in the <100> direction are clearly visible in some parts of the crystal while absent in others that appear equivalent in Bragg geometry. Observation of such differences permits detailed analysis of the processes leading to their formation[2]. Second, the high brightness of a storage ring permits video camera observation of diffraction images in real time. This in turn permits rapid surveys of general aspects of subgrain boundary structure and of large scale crystal strain.

The utilization of a monochromator with a synchrotron storage ring can provide important further advantages, although such a combination is available in the U.S. only on our beam line at the National Synchrotron Light Source[3]. The restriction of diffracting radiation to a narrow spectral band substantially increases the contrast in an image over that obtainable with a white beam as in Figure 5[4-5]. The interpretation of such monochromatic images is far simpler and more certain than the interpretation of images formed with white radiation.

When asymmetric diffraction is employed in the monochromator, two additional benefits can be obtained. First, the beam can be expanded several fold in size to several centimeters in height. With such a beam large crystals can be examined without scanning. Second, the parallelism of the beam is increased by the same factor, bringing the resolution well under one arc second, and approaching a tenth of an arc second depending on the particular monochromator crystal and the energy of the radiation.

All of these advantages together are just now being realized on the National Bureau of Standards Materials Beam Line at the National Synchrotron Light Source at Brookhaven National Laboratory. We turn now to a brief survey of initial results.

II. ILLUSTRATIVE EXAMPLES

A crystal containing distinct grains (which by definition differ in crystallographic orientation) yields conventional x-ray diffraction rocking curves that are broad. Diffraction images of such crystals typically display sharp contrast among the various grains. However, even where the difference in orientation approaches a degree, simultaneous diffraction from more than one grain can be observed if the crystal is suitably oriented with respect to the beam, as has been done in Figure 6. Here, five grains can be distinguished. In such instances, the principal tilt can be accurately determined from the clear displacement of the images of the

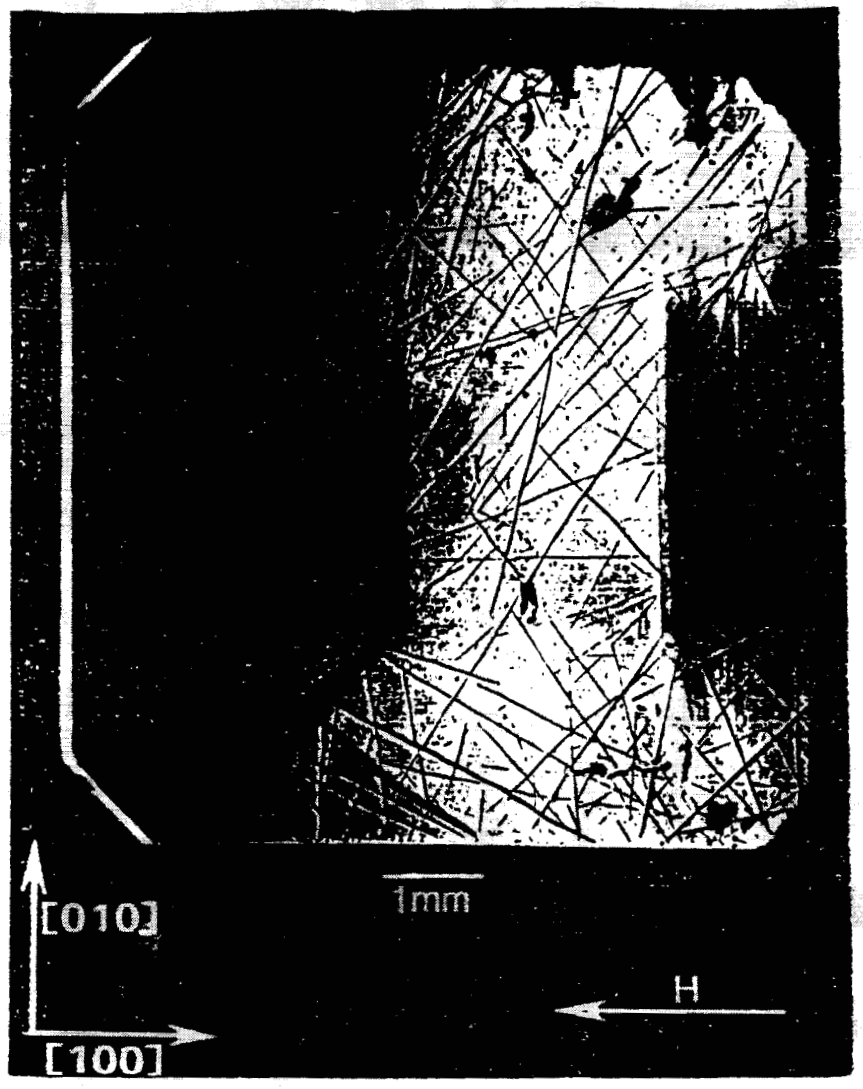

Figure 4. Image of 13.4 keV diffraction in Laue geometry (transmission) from (600) planes of the (001) cut bismuth silicon oxide crystal shown in Figure 1 in diffraction in Bragg geometry.

various grains with respect to one another.

Broad rocking curves can arise also from a different source of imperfection, which, in the absence of images, is sometimes confused with the assumed presence of multiple grains or subgrains.

One such case is shown in Figure 7. The rocking curve for this crystal of cadmium telluride would approach in breadth the curve for the mercuric iodide crystal shown in Figure 6. However, in contrast to the diffraction image of mercuric iodide, the image of cadmium telluride shows no major sharp boundaries separating crystal grains or subgrains. The breadth of the rocking curve in this instance is traceable to relatively gradual, irregular variation either in the lattice constant or in the lattice orientation. Improvement of such crystals will clearly depend on the particular type of crystal imperfection present. Steps taken to reduce the nucleation or propagation of additional grains will be ineffective in improving the quality of crystals whose perfection is limited principally by more subtle inhomogeneity within individual grains, perhaps due to impurities or nonideal stoichiometry.

Sharp subgrain boundaries are observed in high quality crystals, however, as illustrated in Figure 8. Such boundaries cause high contrast in diffraction even when the orientation of the subgrains differs only a few arc seconds in the direction of the beam, as is the case in Figure 8.

Dislocations can be resolved even under unfavorable conditions in which large numbers interact, as is characteristic of undoped gallium

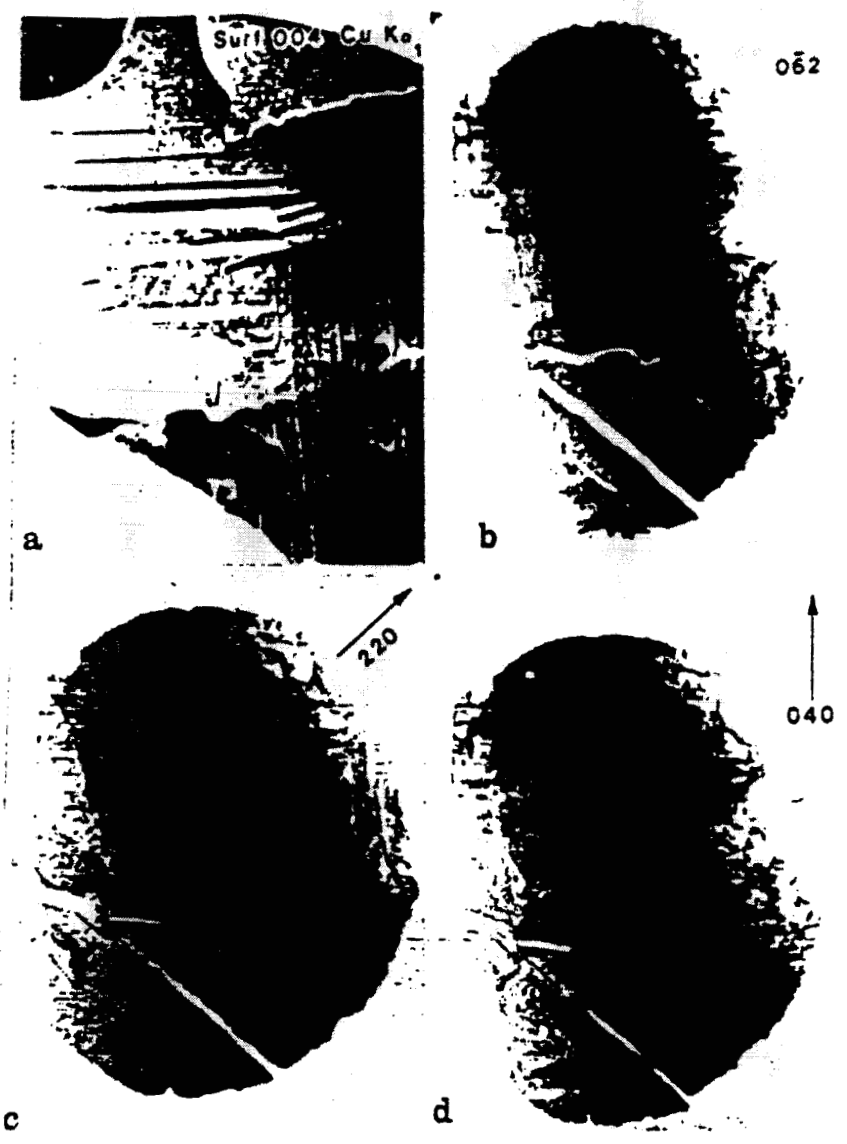

Figure 5. Comparison of monochromatic laboratory diffraction image of iron aluminum crystal with three white beam synchrotron topographs of the same crystal.

arsenide, shown in Figure 9. The orientation of each feature is indicated by the nature of its image. The broad features in the image result from kinematic scattering in the interior of the crystal, while the finer, unbroadened features are diffracted close to the surface.

Other types of structure, clearly related to specific aspects of the growth of a crystal, are visible in observation of indium doped gallium arsenide, as in Figure 10. Geometrical features in a circular region in the center of the boule appear to imply faceted growth in this region. This is surrounded by striations, associated with periodic fluctuation in one or more growth parameters.

An image of the central region of this boule is shown magnified in Figure 11. The rectangular features characteristic of this region are oriented along <110> directions.

III. COMPREHENSIVE UNDERSTANDING

Various strains and other crystallographic irregularities in electrooptic materials can thus be portrayed by diffraction imaging. Through such observations, the role that these defects play can be correlated with specific aspects of device performance. However, also inherent in this technology is the insight that it can provide into the origin of the anomalies and the corresponding potential for their con-

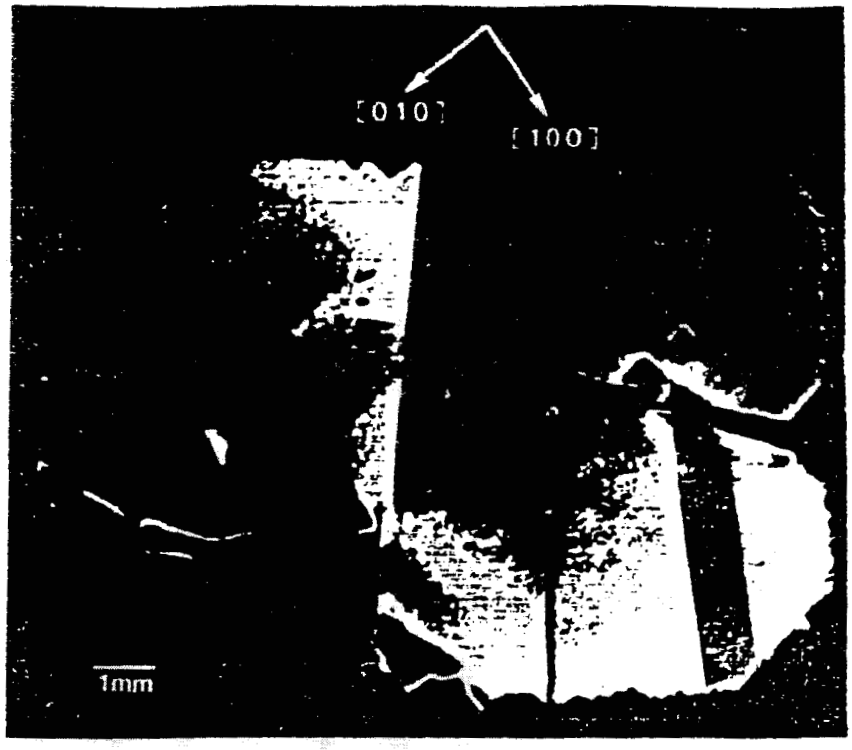

Figure 6. Image of 8 keV diffraction from (1 1 10) planes of a mosaic (001) cut mercuric iodide crystal.

trol where suitable samples are available.

An example of this aspect of monochromatic synchrotron diffraction imaging is a recent study carried out on three slices taken from a single high quality boule of bismuth silicon oxide grown in the [001] direction as shown in Figure 12. The three slices were cut and polished in the c direction, the perimeter retaining the shape that it acquired during growth.

Slice K is shown in Bragg ("reflection") geometry in Figure 1 and in Laue (transmission) geometry in one orientation in Figure 4. Slices E and I are shown in Bragg geometry in Figures 13 and 14, respectively. Slice I is shown in Laue geometry in Figure 15. Slice K is shown in a second orientation in Laue geometry in Figure 16.

Analysis of these diffraction

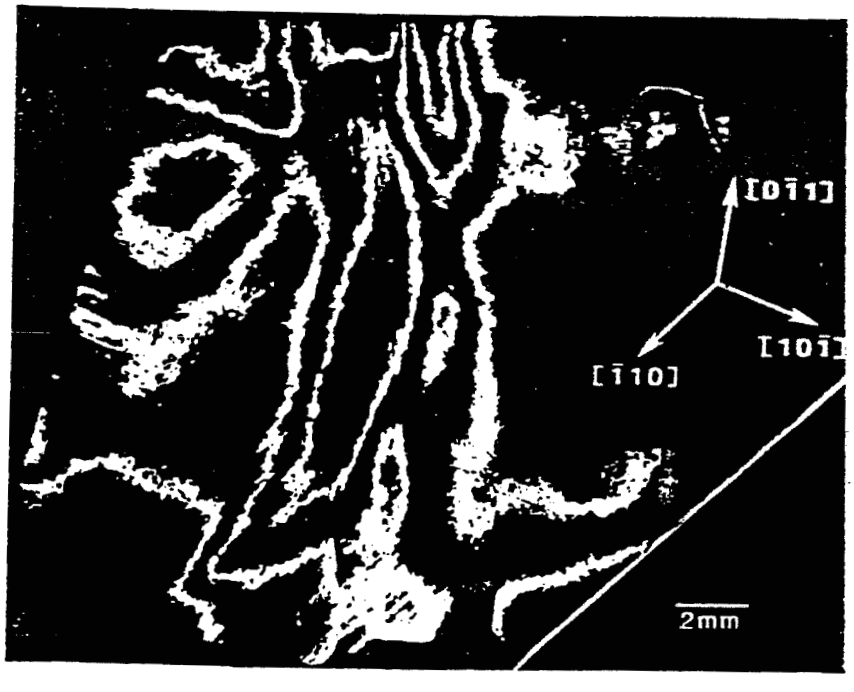

Figure 7. "Contour map" of strains in (111) cut slice of cadmium telluride, recorded by superimposing diffraction from (333) planes of cadmium telluride recorded at three diffraction angles differing by 144 arc seconds.

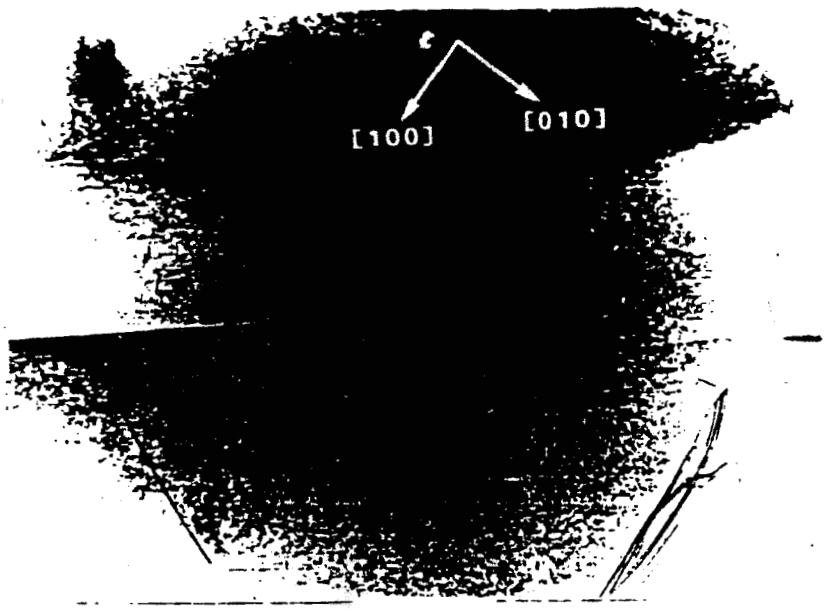

Figure 8. Sharp boundaries separating subgrains differing in orientation by about 2 arc seconds, shown in 8 keV diffraction from (224) planes of a (001) cut undoped gallium arsenide wafer (#3). Also visible are curved regions of strain that produces curved, continuously varying contrast.

images permits us to determine the following sequence of steps in the faceted growth of the boule. Shortly after necking, a small near-(001) growth plane had been established in the center of the growing face. Four peripheral {101} facets had also been formed. These are depicted in Figure 17.

By the time that the boule had grown to the location of slice E, the (0$\bar{1}$1) facet was growing more rapidly than the others, causing it to decrease in area as illustrated in Figure 18. Meanwhile, the central, near-(001) facet was growing nonuniformly. Its growth rate was greater in proximity to the rapidly growing (0$\bar{1}$1) facet, causing the central near-(001) facet to deviate from a precise (001) orientation, observed as strain fringes in the central part of Figure 13.

Between the growth of slice E and that of slice I, the rate of growth of the (0$\bar{1}$1) facet slowed, while the growth of the (101) facet increased, causing a corresponding change in the shape of the related facets as abstracted in Figure 19.

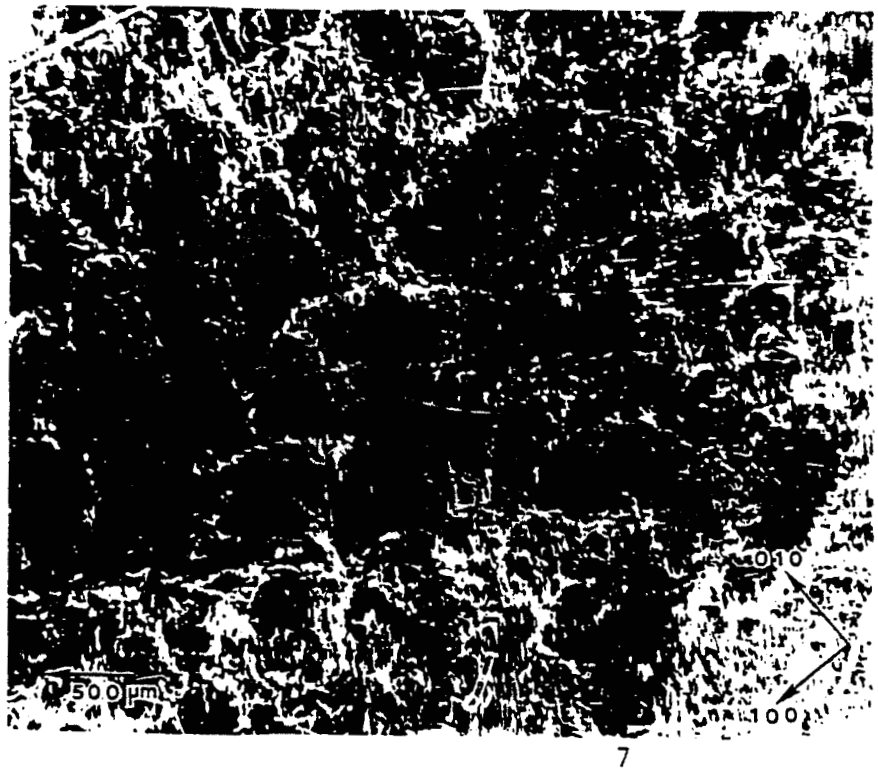

Figure 9. Interacting dislocations observed in 10 keV diffraction in Laue geometry (transmission) from (220) planes of (001) cut undoped gallium arsenide crystal (#5).

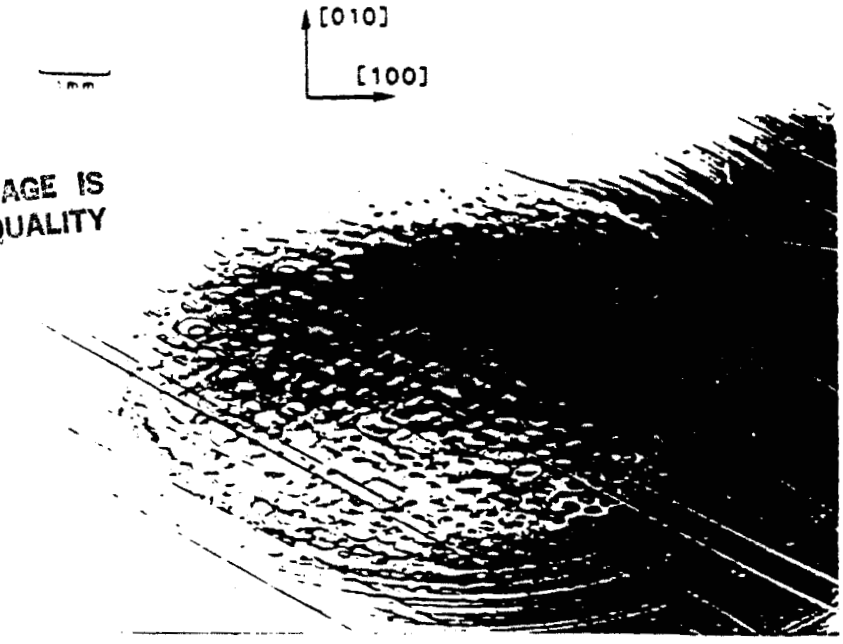

Figure 10. Image of Bragg diffraction at 8 keV from (004) crystal planes of the (001) cut indium doped gallium arsenide wafer shown in Figures 2 and 3 in Laue geometry.

The change in the orientation of the central fringes indicates that the slope of the central near-(001) face underwent a corresponding change.

By the time that the center of the boule had grown to position K, however, growth of the (101) facet had ceased completely, causing a distinctive shape in high strain regions in both slices I and K, and associated with further change in the orientation of the central strain fringes, Figures 19 and 20, respectively.

Specific aspects of this non constant faceted growth model are verified in magnified portions of the diffraction images, Figures 21 and 22. Figure 21 illustrates continuity between fringes observed in the central region and the peripheral striations, supporting the faceted growth model with growth of the central facet at an angle to the (001) plane. Cessation in the growth of the (101) facet while the (011) facet continued to grow is illustrated in Figure 22.

A mathematical model that successfully predicts flow during sta-

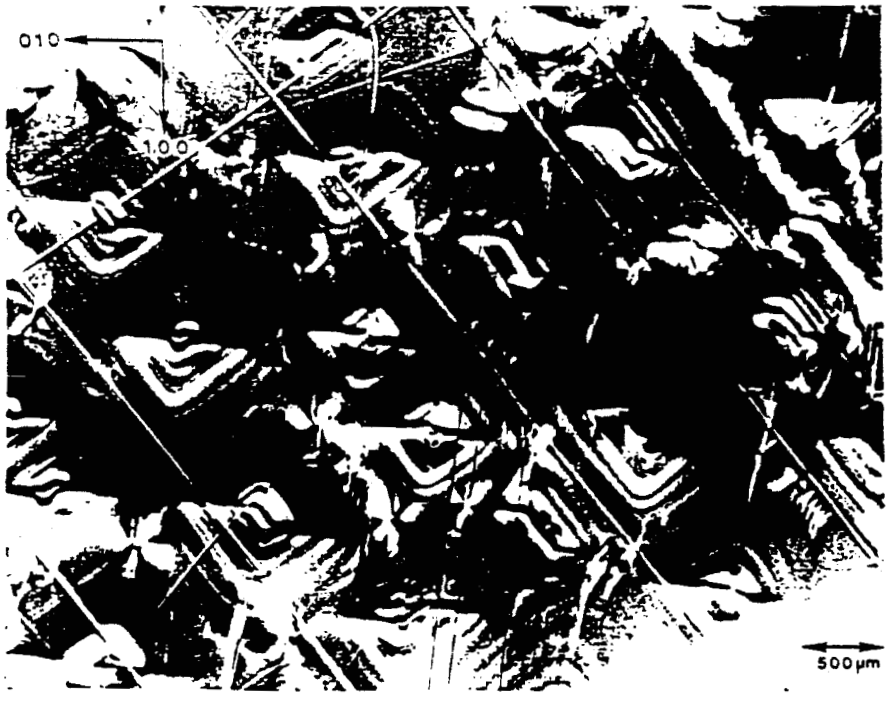

Figure 11. Magnified portion of image of diffraction in Laue geometry at 10 keV from (040) planes of the (001) cut indium doped gallium arsenide crystal shown in Figures 2,3, and 10.

ble Czochralski growth for a flat interface is illustrated in Figure 23. Extension of the general features of this model to faceted growth in Figure 24 illustrates how the asymmetrical faceted growth shown in the diffraction images influences, and in turn is influenced by, changes in the cellular flow, with corresponding changes in the temperature of particular growing regions of the boule and hence the growth morphology.

Variations in materials that can be observed at various stages in the manufacture of devices are illustrated in Figure 25. This shows strains in a piece of lithium niobate indiffused with titanium so that regions of the crystal will guide light to be switched or modulated by electrodes, not yet installed. Such observations can be made first on a virgin material and at various stages in the processing of a device to identify the points at which critical defects are introduced.

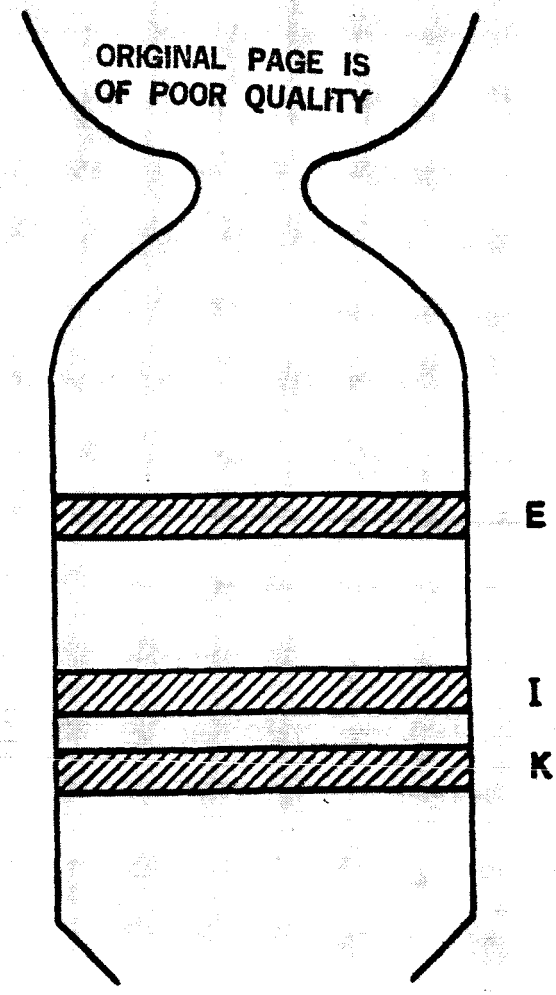

Figure 12. Relative positions of slices taken from a single high quality 8 mm boule of bismuth silicon oxide.

IV. FUTURE DIRECTIONS

While imaging with monochromatic radiation removes ambiguity associated with diffraction by photons with the range of wavelengths in white radiation, another ambiguity in the interpretation nevertheless remains. Contrast in a monochromatic image can be caused either by variation in lattice parameter or by variation in orientation of the crystal lattice. Diffraction from a surface defect surrounded by a perfect crystal is illustrated schematically in Figure 26, in which spatial confusion in the diffracted image is shown to be traceable to dissimilar diffraction angles. A principal consequence of these differing angles is that radiation from such a defect is displaced in the image from the location of the image of the immediately surrounding undisturbed region. Separation of the diffracted radiation from the two sources, defect and surrounding region, and removal of the ambiguity in the source can be accomplished by "out state analysis," through placing an additional diffracting crystal so as to intercept the diffracted image, as illustrated in Figure 27.

Examples of the results of such "out state analysis" are shown in Figures 28 and 29, which picture images of the central region of the indium doped gallium arsenide crystal previously shown in conventional diffraction images Figures 2, 3, and 10.

When the analyzer crystal is set to pass "perfect crystal" diffraction, the contrast between dif-

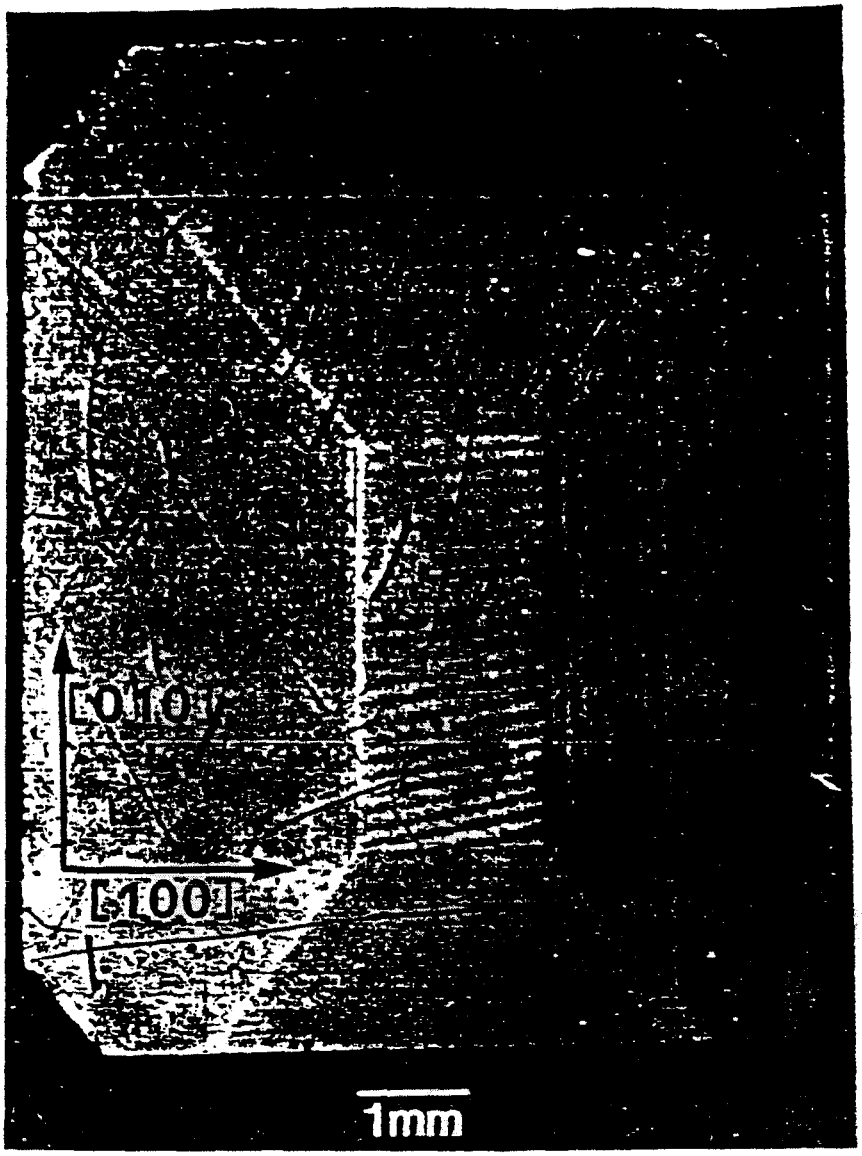

Figure 13. Diffraction image in Bragg geometry of (001) cut slice E of bismuth silicon oxide from (006) planes at 8 keV.

fracting and non diffracting regions is relatively high. This high contrast is caused by the absence of interfering diffraction from defects. When the analyzer crystal is set to discriminate against this "perfect crystal" diffraction, the density of the image is reduced by the lowered diffracted brightness at the "off" angle. Analysis of such simplified images should prove to be more direct and thus less subject to the models employed than is the analysis of conventional diffraction images.

Another opportunity with synchrotron radiation not yet fully exploited is the ability to carry out experiments in real time while observations are made with a video camera. One example whose feasibility has been proved is the observation of changes in the strain in electrooptic crystals as various electromagnetic fields are applied. Strains have been observed in real time in lithium niobate as electrostatic fields are applied. These strains are highly nonuniform, relax with time, and display hysteresis.

In summary, diffraction imaging can provide a great deal of insight into the physics and formation of electrooptic crystals. Through exploitation of this set of opportunities, we expect to expand our understanding of the role of defects and to collaborate with crystal growers in the rapid optimization of these defects, whether increasing the incidence and improving the character of those that can be utilized or reducing those that interfere.

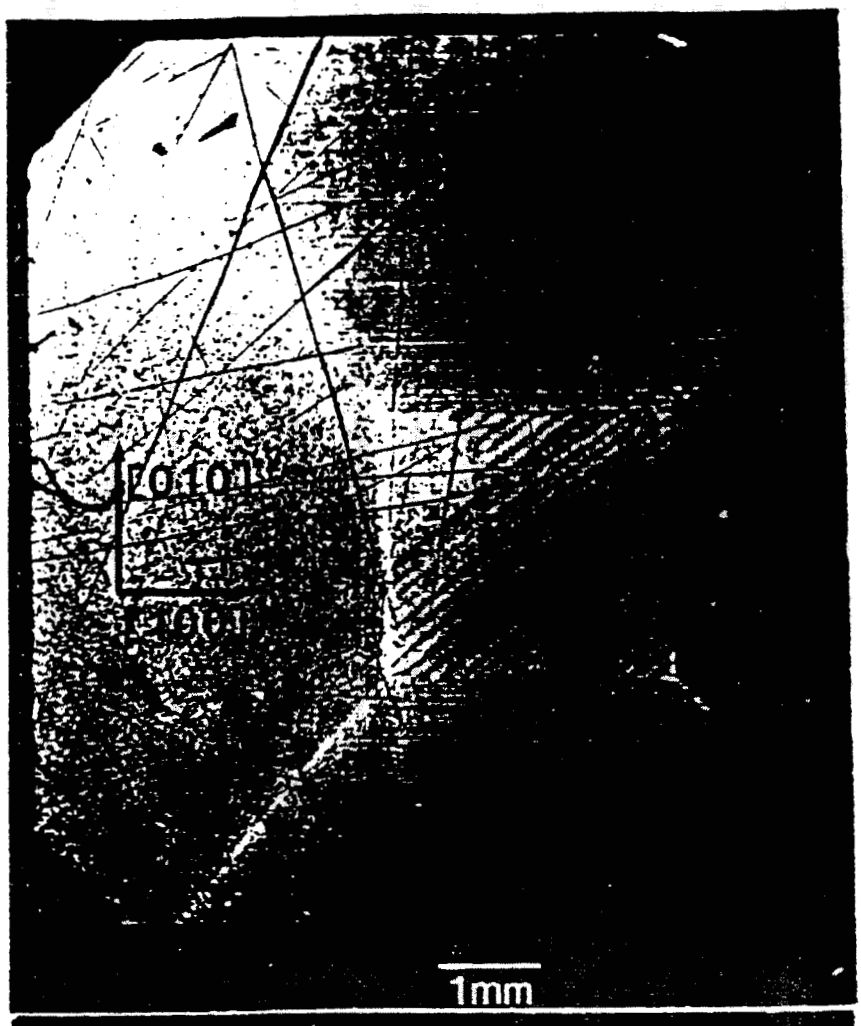

Figure 14. Diffraction image in Bragg geometry of (001) cut slice I of bismuth silicon oxide from (0 0 10) planes at 8 keV.

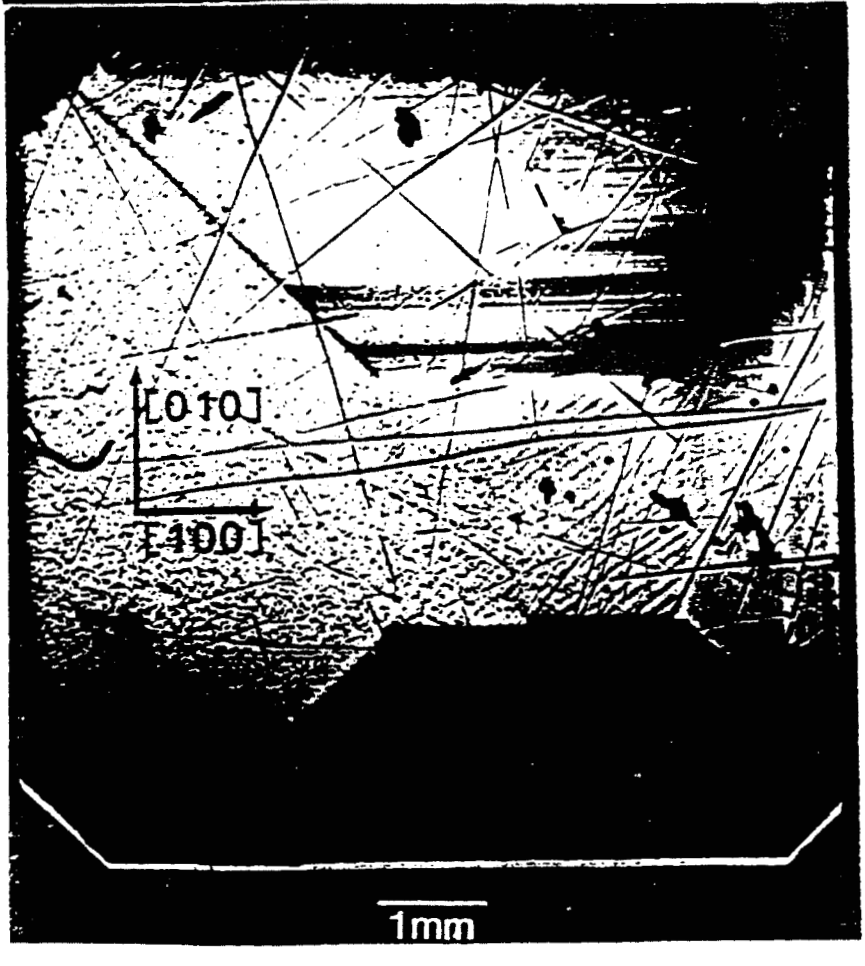

Figure 15. Diffraction image at 13.4 keV in Laue geometry from (0600) planes of bismuth silicon oxide slice I, shown in Bragg geometry in Figure 14.

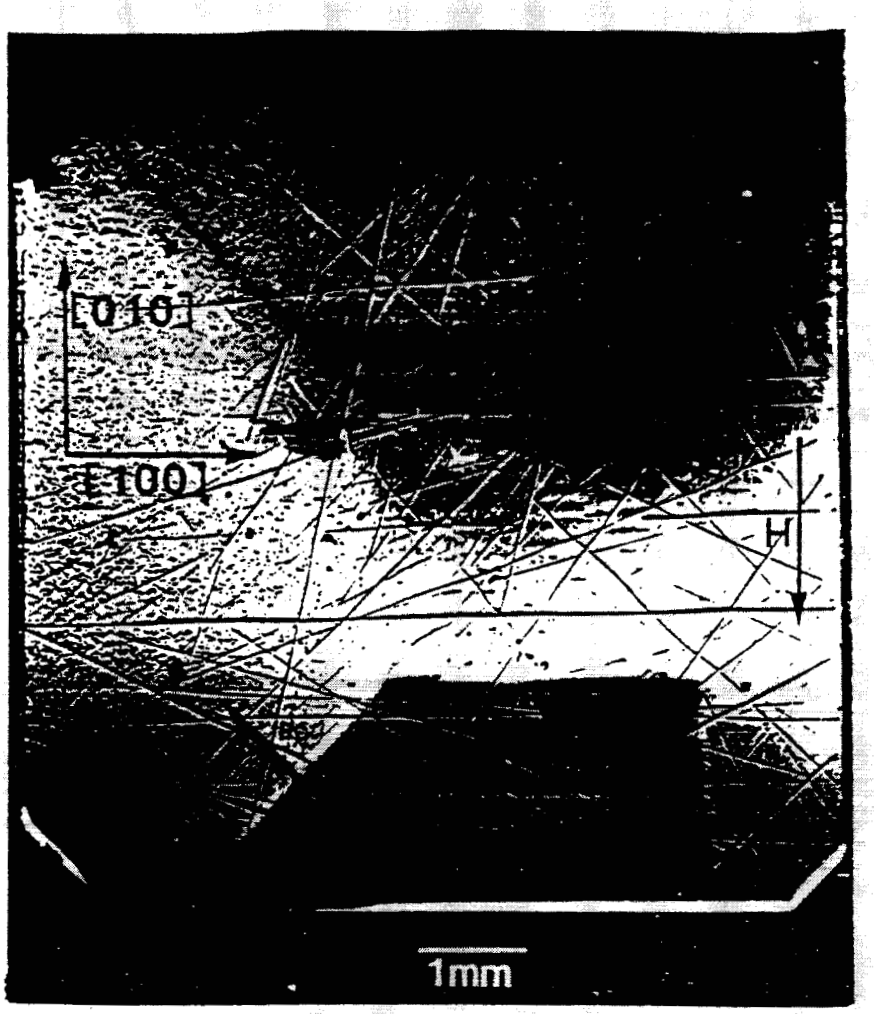

Figure 16. Diffraction image in Laue geometry of bismuth silicon oxide slice K from (060) planes at 13.4 keV. This crystal is shown in Bragg geometry in Figure 1 and in another orientation in Laue geometry in Figure 4.

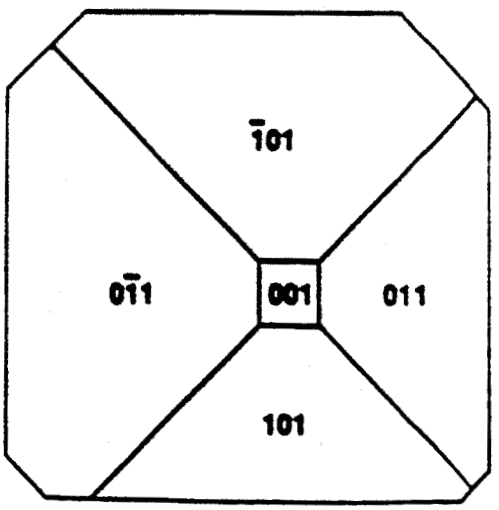

Figure 17. Abstraction of face of growing bismuth silicon oxide boule shortly after initial necking.

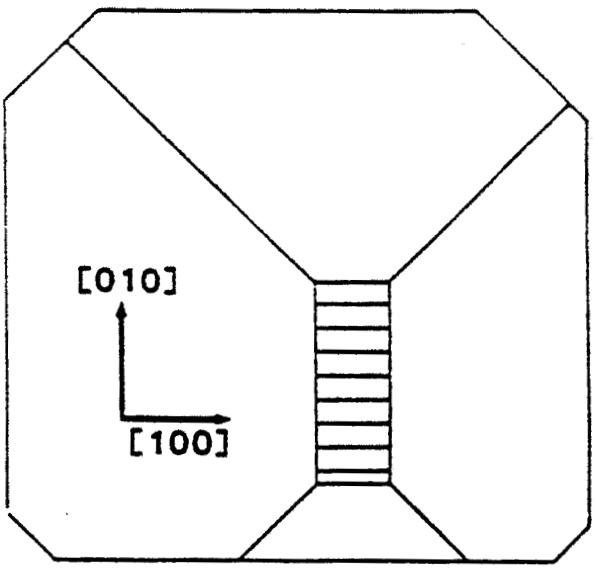

Figure 18. Abstraction of faceted growth of bismuth silicon oxide boule while slice E was being formed.

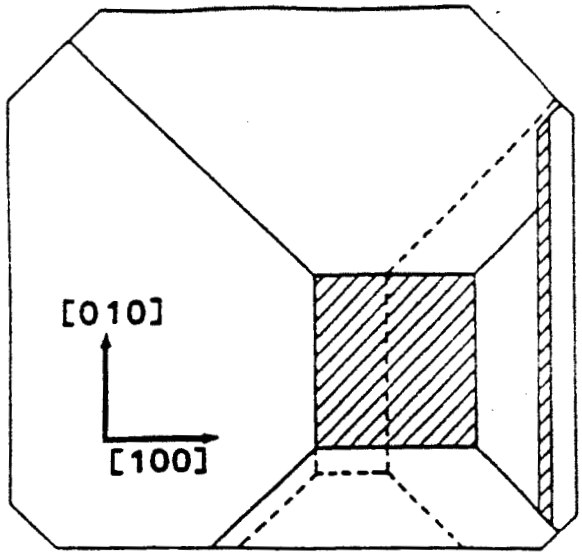

Figure 19. Abstraction of faceted growth of bismuth silicon oxide boule while slice I was being formed.

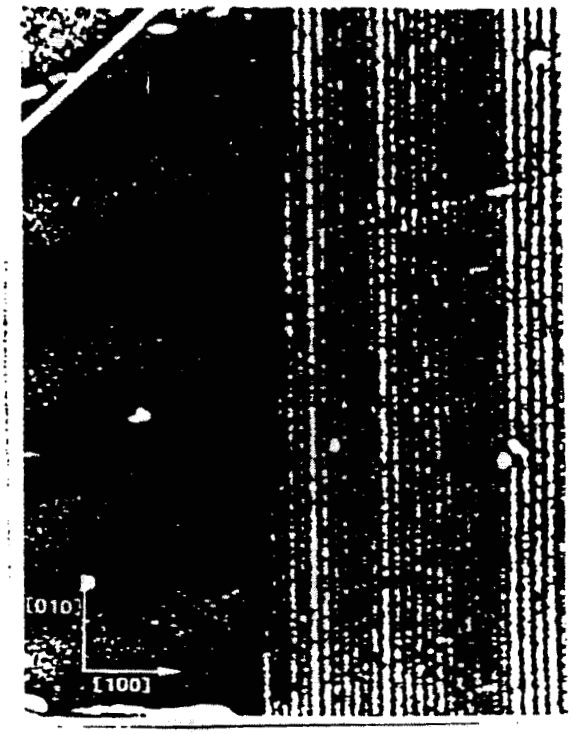

Figure 21. Magnification of region adjacent to the center, in the [100] direction, of a (006) diffraction of slice I in Bragg geometry at 8 keV. This section shows the boundary between the central rectangular near (001) facet growth region containing fringes and the peripheral (101) facet growth.

ACKNOWLEDGEMENTS

The authors acknowledge the support of the U. S. Department of Commerce and of the National Aeronautics and Space Administration, through the Center for the Development of Crystal Growth in Space. The NBS Materials Science synchrotron radiation beam line is located at the National Synchrotron Light Source at Brookhaven National Laboratory, which is supported by the U. S. Department of Energy, Division of Materials Sciences (DOE contract number DE-AC02-76 CH00016).

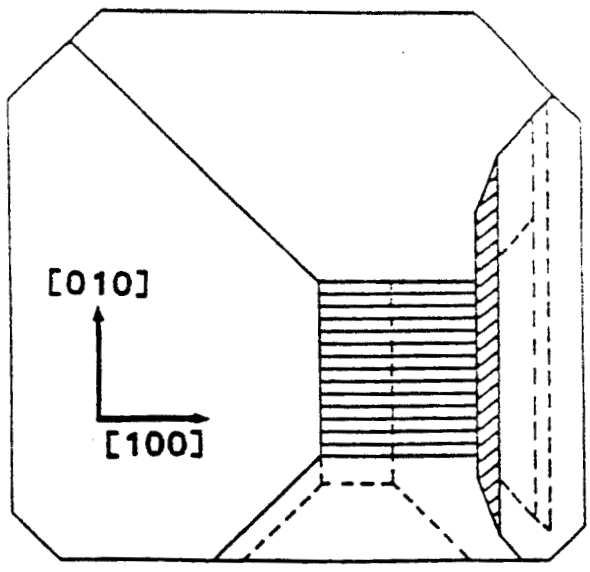

Figure 20. Abstraction of faceted growth of bismuth silicon oxide boule while slice K was being formed.

REFERENCES

1. Present address: Nuclear Research Center, Beer Sheva.

2. Bruce Steiner, Uri Laor, Masao Kuriyama, Gabrielle G. Long, and

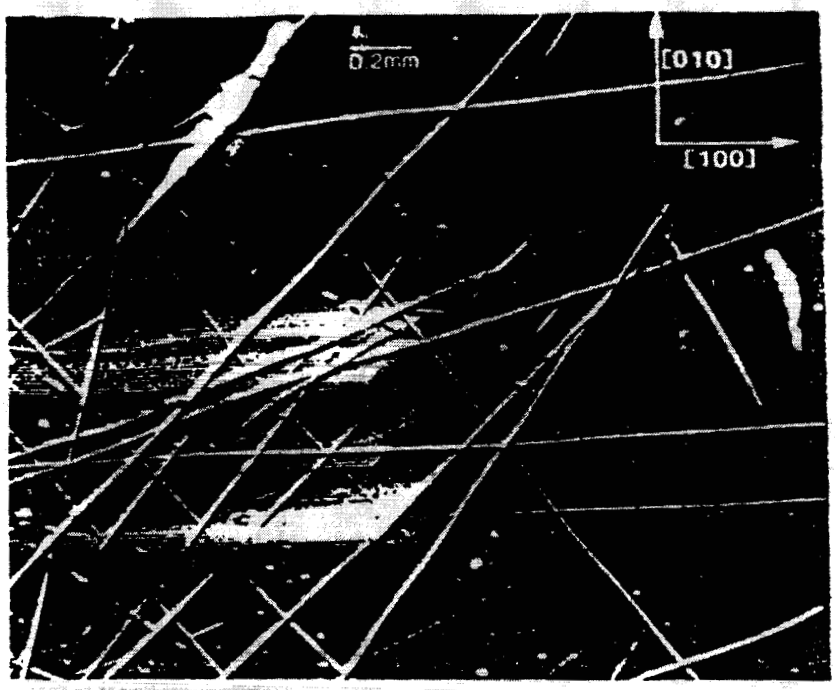

Figure 22. Magnification of the [110] corner region of a (060) diffraction image of slice K in Laue geometry at 13.4 keV. This image shows strains in the [010] direction, and thereby the cessation in the growth of one of the facets while an adjacent facet continued to grow.

Ronald C. Dobbyn, "Diffraction Imaging of High Quality Bismuth Silicon Oxide with Monochromatic Synchrotron Radiation: Implications for Crystal Growth," J. Crystal Growth, 87, 79-100 (1988).

3. R. Spal, R. C. Dobbyn, H. E. Burdette, G. G. Long, W. J. Boettinger, and M. Kuriyama, Nuclear Instruments and Methods 222, 189-192 (1984).

4. Masao Kuriyama, "Applications of Synchrotron Radiation to Materials Science: Diffraction Imaging (Topograph) and Microradiography, in Advanced Techniques for Microstructure Characterization," 1988.

5. W. J. Boettinger, H. E. Burdette, and M. Kuriyama, "White Beam Syn-

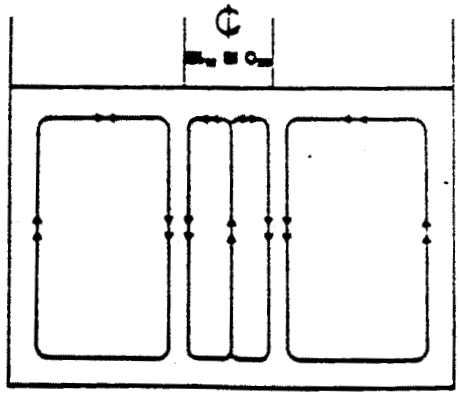

Figure 23. Mathematical model of flow in the bismuth silicon oxide melt for stable flat interface Czochralski growth.

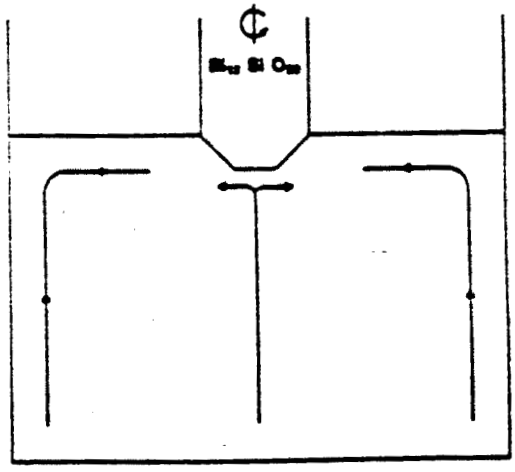

Figure 24. Model of flow in the bismuth silicon oxide melt for faceted interface Czochralski growth. Competition between the two melt currents causes changes in the relative rates of growth of the various facets.

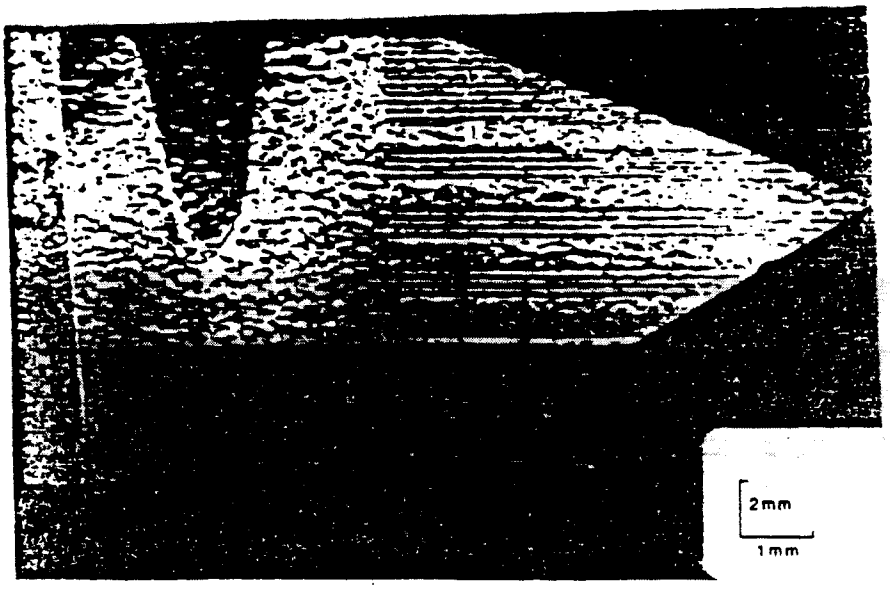

Figure 25. Diffraction image of titanium diffused lithium niobate showing strains caused by this stage in the manufacture of a guided wave device.

chrotron Topography of Metals and Alloys," in "Applications of X-Ray Topographic Methods to Materials Science, "edited by Sigmund Weissmann, Françoise Balibar, and Jean-François Petroff, 283-293 (1984).

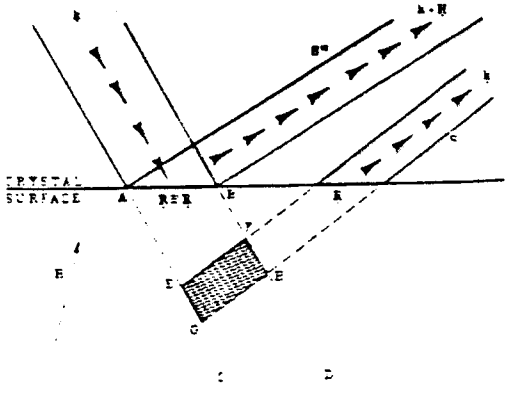

Figure 26. Schematic diagram of sources of image confusion caused by unfortunate combination of defect strain and lattice orientation.

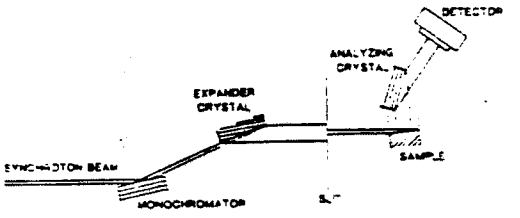

Figure 27. Schematic of experimental arrangement for "out state analysis." Fourth crystal, in addition to two monochromator crystals and the sample being studied, passes the diffracted beam only over a narrow angular range, permitting observation either of defect images or of perfect crystal images without interference from the other type of image.

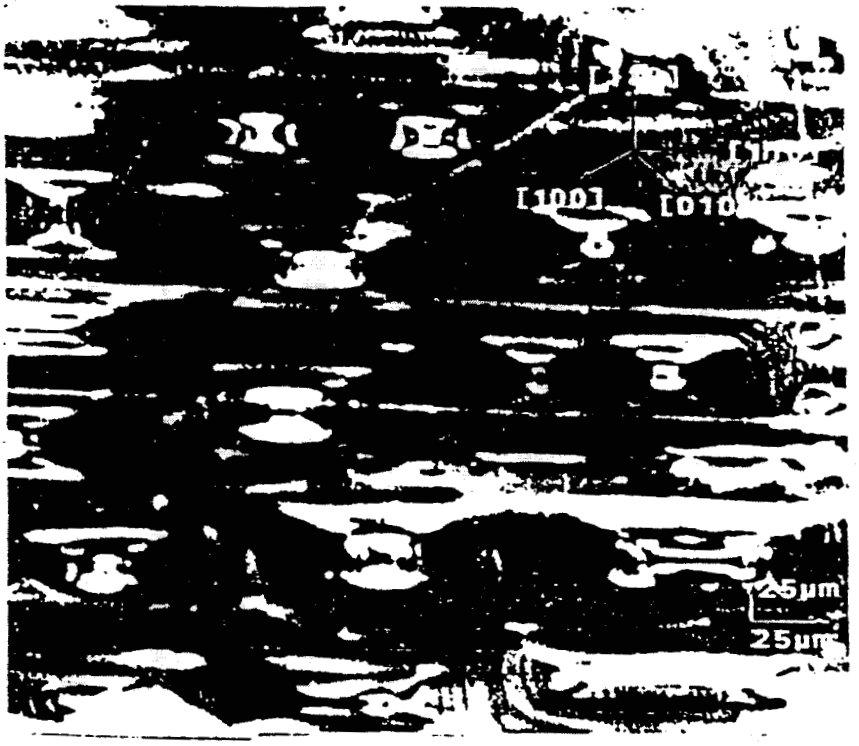

Figure 28. Magnified portion of (004) diffraction image of central portion of (001) cut indium doped gallium arsenide wafer as diffracted by a silicon crystal oriented to pass the "perfect crystal" diffraction and to discriminate against defects.

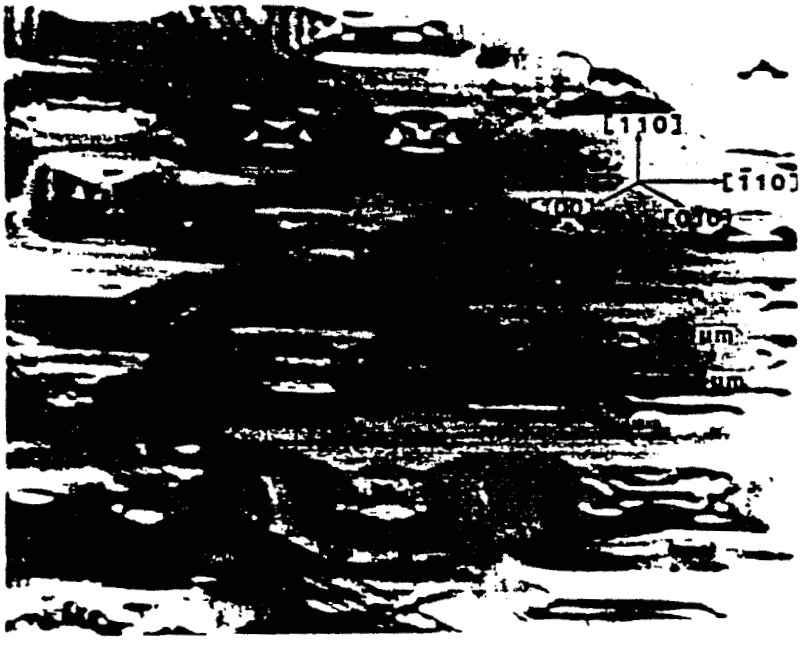

Figure 29. Magnified portion of (004) diffraction image of central portion of (001) cut indium doped gallium arsenide wafer as diffracted by a silicon crystal oriented to pass diffraction from defects and to discriminate against "perfect crystal" diffraction.